Euro. Jnl of Applied Mathematics (2012), *vol.* 23, *pp.* 99–119.
doi:10.1017/S0956792510000380

Conformal mapping techniques for the modelling of liquid crystal devices

A. J. DAVIDSON and N. J. MOTTRAM

Department of Mathematics and Statistics, University of Strathclyde, 26 Richmond Street, Glasgow G1 1XH, UK
email: nigel.mottram@strath.ac.uk

(*Received 23 November 2010; revised 3 December 2010; accepted 6 December 2010; first published online 24 January 2011*)

In this paper, we review a number of uses of conformal mapping techniques for obtaining director profiles of liquid crystals in confined and semi-confined geometries. In particular, we will consider geometries which allow more than one stable state, some of which are of use in bistable displays. These solutions also allow the investigation of the energy of stable states and enable conclusions to be reached as to how such geometries may be optimised for bistable display applications. Such techniques are also able to provide initial configurations for the solution of more complicated situations where numerical methods are used to investigate switching characteristics.

Key words: Liquid crystals, elasticity, conformal mapping, bistablility

1 Introduction

A great deal of research is currently undertaken in the mathematical modelling of liquid crystal displays (LCDs), including devices that can act as low-powered and high-resolution displays. In standard LCDs, the display element requires constant power to retain a static image but in *bistable* LCDs power is only required when switching between different optical states, thus reducing the overall power consumption. This is particularly advantageous in situations where the display does not require to be constantly changed or updated. Bistability in these displays can also have advantages with regards to how the switching of each pixel is electronically addressed, resulting in an increase in the theoretical maximum number of pixels allowed. Ideally, mathematical modelling of the display device could be used to predict optimality (in optical and electronic characteristics) in the design of such devices, mitigating the need for time-consuming and expensive experimental testing. However, the computational resource needed to model most devices means that efficient theory-based optimisation of display qualities such as reduced voltages, high-speed switching and beneficial optical properties, has not been achieved.

To date, several bistable display devices have been proposed and developed [1–10], with a number of these devices reaching the market place in various applications. Most examples of bistable nematic liquid crystal displays involve structural configurations that produce two or more stable states, through which, with the addition of optical elements such as polarisers, can produce the required black and white (or dark and light) states, with some also able to support grey-scale levels.

Current techniques in simulating these devices usually rely on numerical solution methods to solve governing continuum equations of the liquid crystal within the specific geometry [1, 23]. In most of these techniques it is difficult to investigate the numerous stable states since defining initial conditions for each state is non-trivial, particularly if the device in question supports many different stable states.

In this paper we show that by using conformal mapping techniques with classical liquid crystal theory [3,4] we can provide analytical results for both the director profile and total elastic energy for some simple bistable structures. We also investigate more complicated bistable structures and show that a good approximation for the director profile can quickly be determined using conformal mappings.

2 Classical liquid crystal theory

We start by considering a 'classical' theory of liquid crystal elasticity, first developed by Oseen and subsequently by Frank (see de Gennes & Prost) [14]. In this theory there is a single vector-valued macroscopic dependent variable, the director $\mathbf{n}(\mathbf{x})$, which is the average molecular orientation at the point $\mathbf{x}$ in the material. Using a standard angle representation, the director can be written as

$$\mathbf{n} = (\cos\theta\cos\phi, \cos\theta\sin\phi, \sin\theta), \tag{2.1}$$

where θ and ϕ are often termed the zenithal and athimuthal angles respectively, or alternatively the tilt and twist angles. The total free energy of a nematic liquid crystal will then depend on the director and spatial gradients of the director. Oseen–Frank theory uses an application of the calculus of variations to determine minima of this total energy. The free energy could include electrostatic, elastic and thermotropic contributions. However, for simplicity, here we will assume that there are no thermotropic or electrostatic contributions and focus only on the elastic energy. If we assume that, to leading order, the elastic energy depends only on the first derivatives of the director up to quadratic powers, and we consider only terms which obey the inherent symmetries of the nematic phase, then we obtain a relatively simple form of the elastic energy, commonly known as the Frank elastic energy [14],

$$F_{\mathrm{e}} = \int_{\mathscr{V}} \frac{K_{11}}{2}(\nabla\cdot\mathbf{n})^2 + \frac{K_{22}}{2}(\mathbf{n}\cdot\nabla\times\mathbf{n} - q)^2 + \frac{K_{33}}{2}(\mathbf{n}\times\nabla\times\mathbf{n})^2 + \frac{K_{22}+K_{44}}{2}\nabla\cdot[(\mathbf{n}\cdot\nabla)\mathbf{n} - (\nabla\cdot\mathbf{n})\mathbf{n}]\mathrm{d}v, \tag{2.2}$$

where q is the chirality (an inherent twist within the director configuration), $\mathscr{V}$ is the region occupied by the liquid crystal material and K_{11}, K_{22}, K_{33} and K_{44} are the Frank elastic constants [14]. If we now restrict our calculations to consideration of only splay/bend distortions, so that, for instance, the director only lies in the xy-plane and ϕ is independent of z, then the Frank elastic energy becomes

$$F_{\mathrm{e}} = \frac{L}{2}\int_{\mathscr{A}} (K_{11}\cos^2\phi + K_{33}\sin^2\phi)(\nabla\phi)^2\mathrm{d}a, \tag{2.3}$$

https://doi.org/10.1017/S0956792510000380 Published online by Cambridge University Press

where $\mathscr{A}$ is the area in the xy-plane over which the energy density is integrated, $\nabla = (\partial/\partial x, \partial/\partial y)$ and L is the extent of the liquid crystal region in the z-direction. Alternatively, we could consider twist-only distortions where, for instance, the director only lies in the xy-plane and ϕ is independent of y, then the Frank elastic energy becomes

$$F_{\mathrm{e}} = \frac{L}{2}\int_{\mathscr{A}} K_{22}(\nabla\phi)^2 \mathrm{d}a, \tag{2.4}$$

where $\mathscr{A}$ is the area in the xz-plane over which the energy density is integrated, $\nabla = (\partial/\partial x, \partial/\partial z)$ and L is the extent of the liquid crystal region in the y-direction. However, in this paper we restrict attention to the first case above where we have purely splay/bend distortions.

Typically, the elastic constants, K_{11} and K_{33}, are of the same order and so a further simplification is often made by taking a 'one-constant' approximation, $K_{11} = K_{33} = K$. The energy from equation (2.3) then simplifies to

$$F_{\mathrm{e}} = \frac{L}{2}\int_{\mathscr{A}} K(\nabla\phi)^2 \mathrm{d}a. \tag{2.5}$$

Minimisation of this energy [24] provides the differential equation which governs the director angle configuration, Laplace's equation,

$$0 = \nabla^2\phi. \tag{2.6}$$

One well-known technique for solving Laplace's equation in two dimensions involves the use of conformal maps. In this paper we summarise this method and demonstrate, with particularly relevant examples, how such a technique can lead to insights into, and assist numerical simulations of, liquid crystal problems.

Let us consider the xy-plane as the complex plane in which a point in the plane is defined by $z = x + \mathrm{i}\,y$, and assume that we wish to model the configuration of a liquid crystal contained within a fixed region of the plane. For instance we could consider liquid crystal contained within a polygonal region of the plane. Riemann's Mapping Theorem leads to the result that any simply connected 2d domain (except the entire plane) can be mapped onto another simply connected domain. Therefore, the liquid crystal-filled region of the z-plane mentioned above can be mapped onto a simpler domain, say in the $w = u + \mathrm{i}\,v$ plane, using a mapping $w = f(z) = u(x, y) + \mathrm{i}v(x, y)$. For instance, in this paper we will consider the case where the region in the z-plane is transformed onto the upper half plane, i.e. the region of the w plane where $v > 0$.

Suppose $\phi(w)$ is an analytic (i.e. differentiable) function on the w-plane. This is equivalent to saying that the real and imaginary parts of ϕ are harmonic, i.e. a solution to Laplace's equation in the w-plane. Then, the composite function $\phi(f(z))$ is also analytic on the z-plane. This means that, if we can find a solution $\phi(u, v)$ to Laplace's equation in the uv-plane, then the function $\phi(u(x, y), v(x, y))$ is a solution to Laplace's equation in the xy-plane.

We can also calculate how the boundary in the z-plane is mapped to the boundary in the w-plane and ensure that the solution to Laplace's equation in the w-plane, $\phi(u, v)$ satisfies the appropriate boundary conditions, on the appropriate parts of the domain

https://doi.org/10.1017/S0956792510000380 Published online by Cambridge University Press

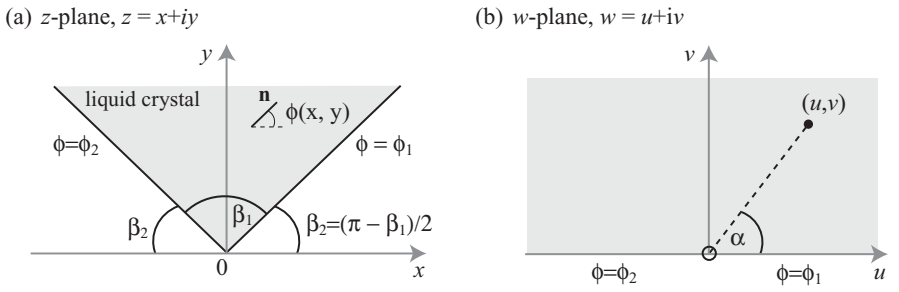

FIGURE 1. The triangular well geometry in (a) is mapped onto the upper half plane in (b).

boundary, so that the function $\phi(u(x, y), v(x, y))$ satisfies the correct boundary conditions in the z-plane. In fact it is not only Dirichlet boundary conditions, where the value of ϕ is fixed on a boundary element, which are unchanged through the mapping from the z-plane to the w-plane. A Neumann boundary condition, where the value of the normal derivative $\partial\phi/\partial v$ is fixed on a boundary element, may also be used since this can be mapped to a similar condition under a conformal mapping. However, the more general Robin boundary condition, where $\partial\phi/\partial v + \lambda\phi = c$ for a prescribed constants λ and c, is not, in general, invariant when a conformal mapping is used.

3 Simple examples

To demonstrate the usefulness of the conformal mapping technique when applied to liquid crystals we will look at a few simple, but relevant, examples for which we can produce analytical results.

3.1 Triangular region

One relatively simple example is that of an infinite region bounded by two substrates at an angle β_1 to each other, as shown in Figure 1(a). We will use this case as a model system to investigate the director structure within a triangular grating structure, similar to the Zenithal Bistable Device [6], which consists of a linear array of triangular wells. In this model system we consider only one well, and it has no upper limit. By using the conformal mapping technique we can produce a director profile for the liquid crystal contained within this region. We can also investigate how the energy is affected when the angle β_1 is changed.

The conformal mapping which maps the trianglular region in Figuare 1(a) to the upper half plane in Figure 1(b) is (Ref. [24])

$$w = u + \mathrm{i}v = z^{\left(\frac{\pi}{\beta_1}\right)} \mathrm{e}^{\left(-\mathrm{i}\pi\frac{\beta_2}{\beta_1}\right)}, \tag{3.1}$$

with $z = x + \mathrm{i}y$ or in expanded form,

$$u = (x^2 + y^2)^{\frac{\pi}{2\beta_1}} \cos\left(\frac{\pi}{\beta_1} \tan^{-1}\left(\frac{y\cos(\beta_2) - x\sin(\beta_2)}{x\cos(\beta_2) + y\sin(\beta_2)}\right)\right), \tag{3.2}$$

https://doi.org/10.1017/S0956792510000380 Published online by Cambridge University Press

and

$$v = (x^2 + y^2)^{\frac{\pi}{2\beta_1}} \sin\left(\frac{\pi}{\beta_1}\tan^{-1}\left(\frac{y\cos(\beta_2) - x\sin(\beta_2)}{x\cos(\beta_2) + y\sin(\beta_2)}\right)\right). \tag{3.3}$$

As each point in the z-plane is mapped onto a distinct point the w-plane, so too are the boundaries. For instance, the point $(x, y) = (0, 0)$ is mapped, using equations (3.2) and (3.3), to $(u, v) = (0, 0)$. The boundary $y = x\tan(\beta_2)$, $x > 0$ is mapped to the line $v = 0$, $u > 0$ and the boundary $y = -x\tan(\beta_2)$, $x < 0$ is mapped to the line $v = 0$, $u < 0$. The boundary conditions in the z-plane can therefore be applied on the appropriate boundaries in the w-plane. Solving Laplace's equation for ϕ in the w-plane with the boundary conditions $\phi = \phi_1$ on $v = 0$, $u > 0$ and $\phi = \phi_2$ on $v = 0$, $u < 0$ gives

$$\phi = \frac{\phi_2 - \phi_1}{\pi}\alpha + \phi_1, \tag{3.4}$$

where $\alpha = \tan^{-1}(\frac{v}{u})$ is the polar angle in the w-plane. We can map this solution back into the geometry in the z-plane by substituting u and v as defined in equations (3.2) and (3.3), respectively. This gives the analytical expression for the director profile in the triangular region as

$$\phi = \frac{\phi_2 - \phi_1}{\beta_1}\tan^{-1}\left(\frac{y\cos(\beta_2) - x\sin(\beta_2)}{x\cos(\beta_2) + y\sin(\beta_2)}\right) + \phi_1. \tag{3.5}$$

For the present situation we will assume that the bounding substrates in Figure 1(a) induce the liquid crystal director to lie parallel to the surface. Therefore, the boundary condition on $y = x\tan(\beta_2)$, $x > 0$ could be $\phi = \phi_1 = \beta_2$. However, because a nematic liquid crystal is non-polar, $\mathbf{n}$ and $-\mathbf{n}$ are equivalent and so the most general form of this boundary condition would be $\phi = \phi_1 = \beta_2 + m\pi$ for any integer m. This is also true for the other substrate at $y = -x\tan(\beta_2)$, $x < 0$, where the condition will be $\phi = \phi_2 = -\beta_2 + n\pi$ where n is an integer. Without loss of generality we may in fact choose boundary values $\phi_1 = \beta_2$ and $\phi_2 = -\beta_2 + n\pi$. The solution in equation (3.5) then becomes,

$$\phi = \frac{n\pi - 2\beta_2}{\pi - 2\beta_2}\tan^{-1}\left(\frac{y\cos(\beta_2) - x\sin(\beta_2)}{x\cos(\beta_2) + y\sin(\beta_2)}\right) + \beta_2, \tag{3.6}$$

where we have used the fact that $\beta_2 = (\pi - \beta_1)/2$.

Here we consider two different sets of boundary conditions that produce different director profiles that are more likely to be observed experimentally in similar manufactured structures. In Figure 2, we have plotted the director structure for the parameter value $\beta_2 = \pi/4$ and the two cases $n = 0$ and 1.

For a bistable device we need to understand how energetically favourable each of these states are. It is clear that the total elastic energy of these states will depend on the apex angle β_1 (or equivalently β_2) and so it will be useful to calculate how the total energy of each state changes with respect to this angle.

Using equations (3.5) and (2.5) we can calculate the total elastic energy, F_e, of the liquid crystal configuration in the triangle. However, care must be taken around defects [22] such as the one at the origin in Figure 1 because, in a director-based model, a disclination

https://doi.org/10.1017/S0956792510000380 Published online by Cambridge University Press

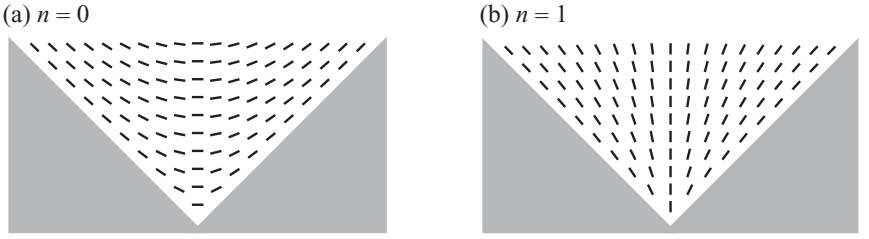

FIGURE 2. Two potential director profiles within a triangular region.

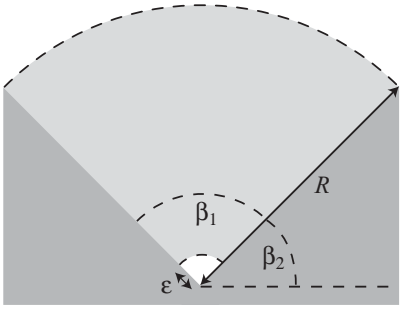

FIGURE 3. Integration of the energy density is performed over the grey area shown, using polar co-ordinates. An area of radius ϵ is not included in the integration to remove the defect from the calculation.

line has infinite energy. Therefore, the energy of a small area around the defect, in this example a circle centred on the defect with radius ϵ, is not included in the calculation (when necessary, ϵ is taken to be small enough as to not affect the relative magnitude of the energies of states). For simplicity we use polar coordinates such that $x = r\cos(\gamma)$ and $y = r\sin(\gamma)$ and integrate over the area shown in Figure 3. In light of the fact that we are interested in the use of triangular gratings, we will consider the finite region bounded by the circular arc $r = R$ to investigate the energy of the liquid crystal within the triangular grating. Using equation (3.5) the total elastic energy, F_e, then becomes

$$\begin{aligned} F_e &= \frac{KL}{2}\int_{\mathscr{A}} (\nabla\phi)^2 \mathrm{d}\mathscr{A} \\ &= \frac{KL}{2}\int_{\epsilon}^{R}\int_{\beta_2}^{\pi-\beta_2} \frac{1-\sin(2\gamma)}{r}\left(\frac{\phi_1-\phi_2}{\beta_1}\right)^2 \mathrm{d}\gamma\,\mathrm{d}r \\ &= \frac{KL}{2}\frac{(\phi_1-\phi_2)^2}{\beta_1}\ln\left(\frac{R}{\epsilon}\right), \end{aligned} \tag{3.7}$$

where limits of integration, R and ϵ, are indicated in Figure 3. With $\phi_1 = \beta_2 = (\pi - \beta_1)/2$ and $\phi_2 = -\beta_2 + n\pi = -(\pi - \beta_1)/2 + n\pi$, as before, the energy is,

$$F_e = \frac{KL((1-n)\pi - \beta_1)^2}{2\beta_1}\ln\left(\frac{R}{\epsilon}\right). \tag{3.8}$$

https://doi.org/10.1017/S0956792510000380 Published online by Cambridge University Press

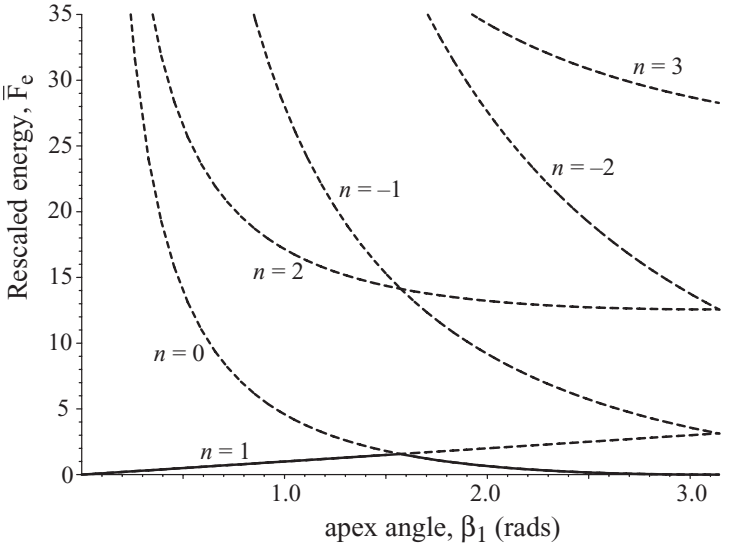

FIGURE 4. Rescaled energy as a function of apex angle for different values of n. With apex angle less that $\pi/2$, the state in Figure 2(b) is energetically favourable but for larger apex angles the state shown in Figure 2(a) is favourable. Solid lines: lowest energy solutions, dashed lines: higher energy solutions.

We may rescale energy in the following way

$$\bar{F}_e = \frac{2}{KL\ln\left(\frac{R}{\epsilon}\right)}F_e = \frac{((1-n)\pi-\beta_1)^2}{\beta_1}. \tag{3.9}$$

In Figure 4 we have plotted the rescaled energy $\bar{F}_e$, for a number of values of n, as the angle β_1 varies. From this we can see that if the angle β_1 is less that $\pi/2$ then state $n = 1$ is energetically favoured. When $\beta_1 > \pi/2$ state $n = 0$ is energetically favourable. States with $n > 1$ are always higher energy states. This type of result is useful when designing a bistable display as it is usually a requirement that both states are of similar or equal energy (i.e. for equal energy we would use $\beta_1 = \pi/2$). Modifications of this analysis, to include pretilts on the solid substrates or for a rotated corner region (in order to model a skew grating), are relatively simple to undertake.

3.2 Rectangular channel grating

Another application of this method is in the situation where liquid crystal material fills a channel of rectangular cross-section, as shown in Figure 5(a) with three walls exhibiting planar anchoring (i.e. the director lies parallel to the boundary). In the analysis that follows this region is unbounded as y increases. In reality there will be an upper surface, some distance h from the base, and will mimic the existence of an upper surface by considering only the elastic energy of the liquid crystal within the region $-a/2 < x < a/2$, $0 < y < h$. This type of device geometry has been investigated in Ref. [8]. The conformal

https://doi.org/10.1017/S0956792510000380 Published online by Cambridge University Press

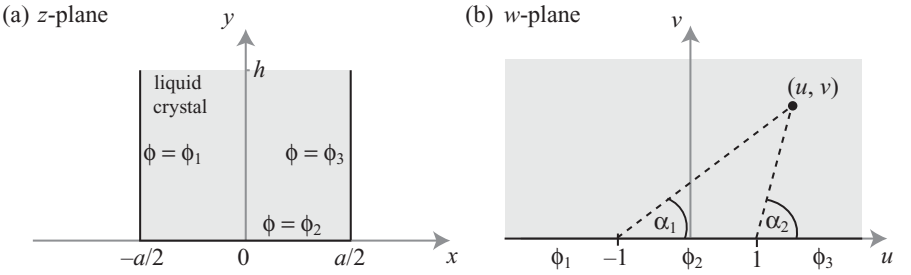

FIGURE 5. The rectangular well geometry in (a) is mapped onto the upper half plane in (b).

mapping which transforms the rectangular well to the upper half plane is

$$w = u + \mathrm{i}v = \sin\left(\frac{\pi}{a}(x + \mathrm{i}y)\right). \tag{3.10}$$

Here the boundaries of the rectangular well in the z-plane are mapped onto the u-axis in the w-plane with the same boundary conditions, as shown in Figure 5. We note that the corners of the well in the z-plane at $x = \pm a/2$ and $y = 0$ map into $u = \pm 1$ on the w-plane.

Solving Laplace's equation for ϕ in the w-plane with the boundary conditions as shown in Figure 5(b) gives

$$\phi = \left(\frac{\phi_1 - \phi_2}{\pi}\right)\tan^{-1}\left(\frac{v}{u+1}\right) + \left(\frac{\phi_2 - \phi_3}{\pi}\right)\tan^{-1}\left(\frac{v}{u-1}\right) + \phi_3. \tag{3.11}$$

Substituting for u and v from the real and imaginary parts of equation (3.10) into equation (3.11) gives the resulting solution for the director profile in the rectangular well as

$$\begin{aligned}\phi = &\left(\frac{\phi_1 - \phi_2}{\pi}\right)\tan^{-1}\left(\frac{\cos\left(\frac{x\pi}{a}\right)\sinh\left(\frac{\pi y}{a}\right)}{\sin\left(\frac{x\pi}{a}\right)\cosh\left(\frac{\pi y}{a}\right)+1}\right)\\ &+\left(\frac{\phi_2 - \phi_3}{\pi}\right)\tan^{-1}\left(\frac{\cos\left(\frac{x\pi}{a}\right)\sinh\left(\frac{\pi y}{a}\right)}{\sin\left(\frac{x\pi}{a}\right)\cosh\left(\frac{\pi y}{a}\right)-1}\right)+\phi_3.\end{aligned} \tag{3.12}$$

As in the previous section, using different values of ϕ_1, ϕ_2 and ϕ_3 can produce different director profiles within the rectangular well. Figure 6 shows solutions with boundary conditions: (a) $\phi_1 = -\pi/2$, $\phi_2 = 0$ and $\phi_3 = \pi/2$, (b) $\phi_1 = \pi/2$, $\phi_2 = 0$ and $\phi_3 = \pi/2$ and (c) $\phi_1 = \pi/2$, $\phi_2 = 0$ and $\phi_3 = -\pi/2$.

It is possible, using crossed polarisers, for these director states to produce different optical states when light is transmitted through the device. We note here that there are other, higher energy, director states, as in the previous section, but we omit these states for conciseness and due to their irrelevance to real devices. There is also a director configuration which is obtained by simply reflecting state (b) about the vertical axis, and therefore has the same energy as state (b). Using equations (3.7) and (3.12) we can then

https://doi.org/10.1017/S0956792510000380 Published online by Cambridge University Press

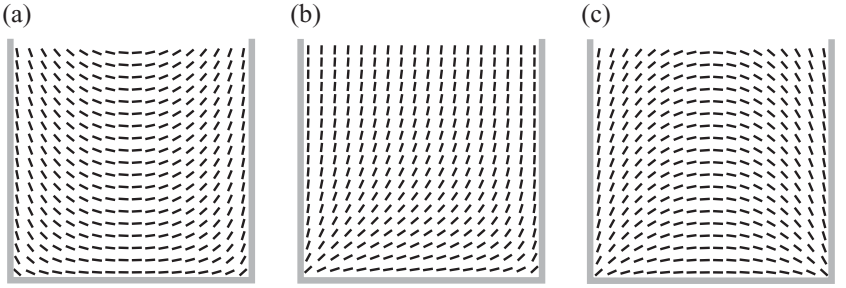

FIGURE 6. Three potential director profiles that occur in the rectangular well geometry.

write the elastic energy of each of these states,

$$F_{\mathrm{e}}{}^{(a)} = F_{\mathrm{e}}{}^{(c)} = \frac{\pi^2 K L}{2a^2} \int_0^h \int_{-a/2}^{a/2} \frac{\cosh^2\left(\frac{\pi y}{a}\right) - \cos^2\left(\frac{\pi x}{a}\right)}{\cosh^2\left(\frac{\pi y}{a}\right) - \sin^2\left(\frac{\pi x}{a}\right)} \,\mathrm{d}x\,\mathrm{d}y \tag{3.13}$$

$$F_{\mathrm{e}}{}^{(b)} = \frac{\pi^2 K L}{2a^2} \int_0^h \int_{-a/2}^{a/2} \frac{1}{\cosh^2\left(\frac{\pi y}{a}\right) - \sin^2\left(\frac{\pi x}{a}\right)} \,\mathrm{d}x\,\mathrm{d}y, \tag{3.14}$$

where, as before, L is the extent of the channel in the z-direction. We therefore find that the energies of two of the states, (a) and (c) in Figure 6, are equal and, although the energy integrals above may not be analytically computed, it is possible to make progress when we consider the difference in energies, $\Delta F = F_{\mathrm{e}}{}^{(a)} - F_{\mathrm{e}}{}^{(b)}$. Because of the singularities at the corners of the region we must again remove a small area from around the defect from the integration region. If we therefore remove the areas $-a/2 < x < -a/2 + \epsilon$, $0 < y < \epsilon$ and $a/2 - \epsilon < x < a/2$, $0 < y < \epsilon$, the rescaled energy difference $\Delta\bar{F} = \frac{2}{\pi^2 KL}\Delta F$ can be computed as a Taylor series in the small parameter ϵ,

$$\Delta\bar{F} = -\lambda + \frac{2}{\pi}\ln\left(\cosh\left(\pi\lambda\right)\right) + O\left(\epsilon\right), \tag{3.15}$$

where $\lambda = h/a$ is the aspect ratio of the integration region. If we take only the leading order term in equation (3.15), and consider the point at which the difference in energies is zero, we obtain the following equation for the value of the aspect ratio for which the energies are equal,

$$\left(\mathrm{e}^{\frac{\pi\lambda}{2}}\right)^4 - 2\left(\mathrm{e}^{\frac{\pi\lambda}{2}}\right)^3 + 1 = 0. \tag{3.16}$$

The only real non-zero solution for the aspect ratio is then,

$$\lambda = \frac{2}{\pi}\ln\left(\frac{1}{3}\left((19 + 3\sqrt{(33)})^{(1/3)} + 4(19 + 3\sqrt{(33)})^{-(1/3)} + 1\right)\right) = 0.38794 = \lambda_c. \tag{3.17}$$

The energies (suitably rescaled as before) may also be calculated numerically, and are shown in Figure 7, where the value of $\epsilon/a = 10^{-4}$ has been used for the lateral dimension of the regions near to the defects which have been removed from the region of integration. The difference between the two energies in Figure 7 is given by the expression in equation (3.15).

https://doi.org/10.1017/S0956792510000380 Published online by Cambridge University Press

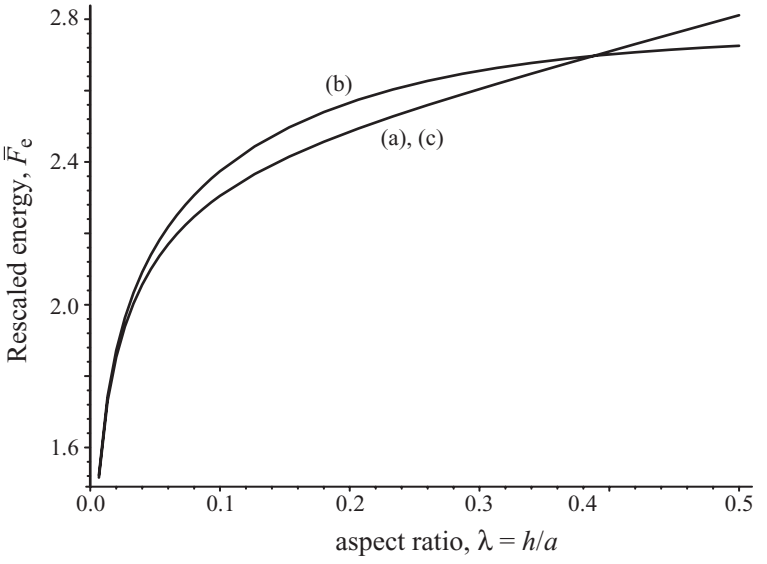

FIGURE 7. Rescaled elastic energy of the director states from Figure 6 as the the aspect ratio (height/width) is varied.

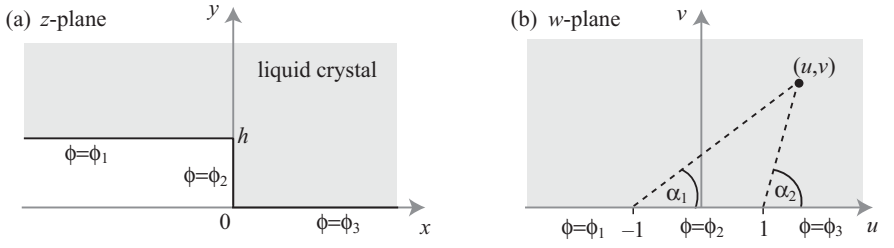

FIGURE 8. The geometry in (a) is mapped onto the upper half plane in (b) using equation (3.18).

From Figure 7 we can see that for channels in which the height is approximately a third or less of the width ($\lambda < \lambda_c$) the states shown in Figure 6(a) or (c) are most likely to be observed, whereas for taller channels, where $\lambda > \lambda_c$ we would expect the state shown in Figure 6(b) to be observed. Although in real devices the upper substrate or a region of liquid crystal above $y = h$ may affect the relative energies of these states, it is useful to consider this simplified system since it provides an initial estimate against which experimental measurements can be compared or initial testing of a device can be developed.

3.3 Substrate step

It is not always possible to obtain an explicit form of the conformal map $w = f(z)$ and for the case of a step of height h in the lower boundary, as shown in Figure 8, only the

https://doi.org/10.1017/S0956792510000380 Published online by Cambridge University Press

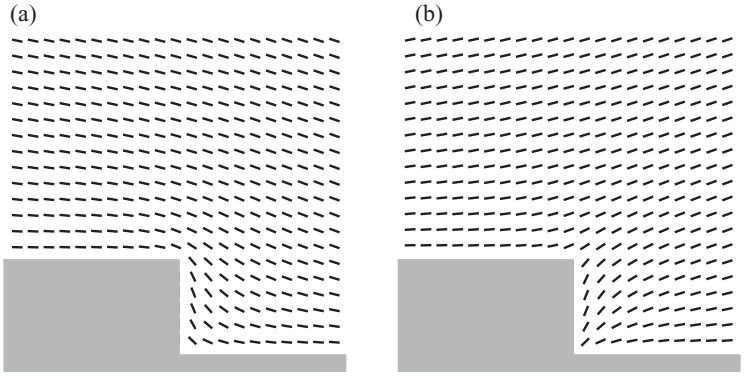

FIGURE 9. Director profiles of the two different states for the step geometry.

inverse conformal mapping can be expressed explicitly [12],

$$z = f^{-1}(w) = \frac{h}{\pi}((w^2 - 1)^{1/2} + \cosh^{-1}(w)). \tag{3.18}$$

It is simple to see however that, for the mapping defined by equation (3.18), the corners of the step in the z-plane: (0,0) and (0,h), map to (1,0) and (−1,0) in the w-plane, respectively. The boundary $x < 0$, $y = h$ maps onto $v = 0$, $u < -1$, the boundary $x = 0$, $0 < y < 1$ maps onto $v = 0$, $-1 < u < 1$ and the boundary $x > 0$, $y = 0$ maps onto $v = 0$, $u > 1$. In the w-plane, therefore, the length h is not present, a fact that will subsequently be of use.

Solving Laplace's equation in the w-plane gives,

$$\phi = \left(\frac{\phi_1 - \phi_2}{\pi}\right) \tan^{-1}\left(\frac{v}{u+1}\right) + \left(\frac{\phi_2 - \phi_3}{\pi}\right) \tan^{-1}\left(\frac{v}{u-1}\right) + \phi_3, \tag{3.19}$$

where u and v are defined implicitly by the expression

$$x + \mathrm{i}y = \frac{1}{\pi}(((u + \mathrm{i}v)^2 - 1)^{1/2} + \cosh^{-1}(u + \mathrm{i}v)). \tag{3.20}$$

Although little can be done analytically at this point we may still compute the director configuration at any point in the z-plane: specifying x and y, we can find solutions u and v using equation (3.20) which are then entered into equation (3.19) to determine ϕ. Although this process, in particular finding the solution of equation (3.20), must be performed numerically, a higher degree of accuracy can be obtained for relatively little computational resource compared to solving the full two-dimensional problem by, for instance, a finite element implementation.

Figure 9 shows the results of this process, producing the director profiles for two different sets of boundary conditions (a) the boundary values $\phi_1 = 0$, $\phi_2 = -\pi/2$ and $\phi_3 = 0$ and (b) the boundary values $\phi_1 = 0$, $\phi_2 = \pi/2$ and $\phi_3 = 0$. These two stable configurations have in fact been investigated previously [27], using a more computationally intensive numerical method, and it has been shown experimentally that these states are stable and the application of an electric field can switch between the two states.

https://doi.org/10.1017/S0956792510000380 Published online by Cambridge University Press

The energy integral for the substrate step geometry can be calculated in a similar fashion as in previous sections. We note however that the integration may also be performed in the w-plane through a transformation of variables,

$$\bar{F}_{\mathrm{e}} = \frac{2}{KL} F_{\mathrm{e}} = \int_{\mathscr{A}_{xy}} (\nabla\phi(x,y))^2 \,\mathrm{d}x\,\mathrm{d}y = \int_{\mathscr{A}_{uv}} (\nabla\phi(u,v))^2 \,\left|\det(J_{\bar{f}}(x,y))\right| \,\mathrm{d}u\,\mathrm{d}v, \quad (3.21)$$

where $\bar{f} = (\mathrm{Re}f(z), \mathrm{Im}f(z))$ is the vector function which maps the point (x,y) to the point (u,v) and $J_{\bar{f}}$ is the Jacobian of the transformation. Integrating in the w-plane may sometimes be easier although care must be taken when considering the region of integration, particularly if areas surrounding defects are to be removed before integrating. A suitable defect area in the z-plane, i.e. a circular region, will be mapped to a non-circular region in the w-plane. In the present situation we will not perform the integration but simply consider the integrand $(\nabla\phi(u,v))^2$. For the two sets of boundary condition considered above, $\phi_1 = 0$, $\phi_2 = \pm\pi/2$ and $\phi_3 = 0$, the integrand in both cases reduces to

$$(\nabla\phi(u,v))^2 = \frac{1}{(u^2+v^2+1)^2 - 4u^2}. \quad (3.22)$$

Therefore, since the Jacobian is only dependent on the mapping in equation (3.20), the energies of the two states in Figure 9 will be equal.

One further observation can be made. Given that the mapping f^{-1} can be written as $f^{-1} = hg^{-1}$, with g^{-1} independent of the step height h, the Jacobian in equation (3.21) will be inversely proportional to h, and the energy of each state will be of the form $\bar{F}_{\mathrm{e}} = c/h$ for some constant c. This result is consistent with the approximation of the step configuration to the director profile produced by two defects placed at the two corners in the system, two positive defects for case (a) in Figure 9 and two negative defects for case (b). As h increases the defects at the corners move apart and, since two positive (or two negative) defects repel each other, the elastic energy of the system reduces. The reduction at a rate proportional to $1/h$ is consistent with standard results (see for instance Ref. [14]).

4 Schwarz–Christoffel transformation

Unfortunately, for more complex geometries it is more difficult to produce analytical results. For many cases the relevant mapping is the *Schwarz–Christoffel* transformation [12], used to map polygonal regions to the upper half-plane. For example, for the region enclosed by the geometry shown in Figure 10(a) which has internal angles $\alpha_1,\ldots,\alpha_n$ at vertices $z_1,\ldots,z_n$ respectively, we require a map from this geometry from the upper-half plane shown in Figure 10(b), where the points $z_1,\ldots,z_n$ need to map onto $u_1,\ldots,u_n$ respectively. The inverse map, which maps the interior of the upper half-plane in the w-plane onto the polygon in the z plane is given by the Schwarz–Christoffel transformation

$$z = A\int (w-u_1)^{\frac{\alpha_1}{\pi}-1}(w-u_2)^{\frac{\alpha_2}{\pi}-1}\ \ldots\ (w-u_n)^{\frac{\alpha_n}{\pi}-1}\mathrm{d}z + B, \quad (4.1)$$

where A and B are complex constants.

https://doi.org/10.1017/S0956792510000380 Published online by Cambridge University Press

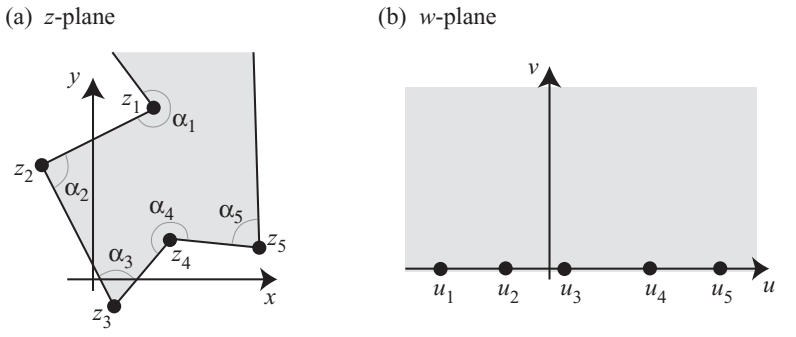

FIGURE 10. The Schwarz–Christoffel transformation maps polygons in the z-plane onto the upper half w-plane.

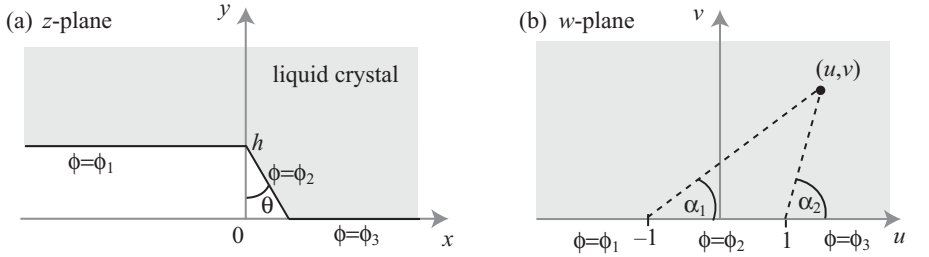

FIGURE 11. The geometry in (a) is mapped onto the upper half plane in (b) using equation (4.1).

In a similar way as in the last section, the main difficulty with this transformation is that, with the exception of some special cases, the points $u_1, \ldots, u_n$ cannot be computed analytically and only the inverse mapping can be written explicitly. Three of the points may be set arbitrarily and the remaining $n-3$ points can be found by solving a system of non-linear equations. Once this is done, the constants A and B can be found by examining the size and location of the polygon (where A determines the size of the polygon and B its location), and $z(w)$ and its inverse can be computed numerically [12, 15]. Although this process involves a certain level of numerical approximation it is, as in the previous section, computationally efficient when compared to a full solution to Laplace's equation (or a more accurate but more complicated non-linear differential equation modelling the director configuration) in the original polygonal geometry.

In the following sections we will consider a number of geometries which have been previously considered experimentally and may be of industrial relevance. We demonstrate how the Schwarz–Christoffel transformation may be used as an alternative to solving a more complicated theoretical model and may be able to aid optimisation of devices.

4.1 Titled step geometry

The step geometry described in the previous section can be generalised to a tilted step, as shown in Figure 11, and was indeed considered in [27]. In this case the mapping is more complicated than the last section and is in the form of the Schwarz–Christoffel mapping

https://doi.org/10.1017/S0956792510000380 Published online by Cambridge University Press

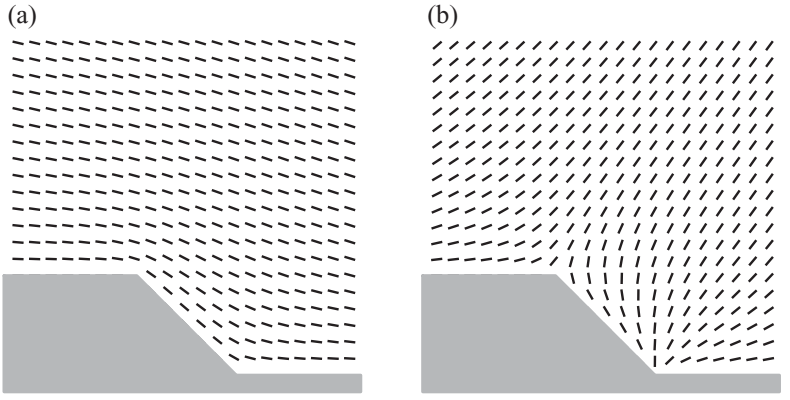

FIGURE 12. The director profile produced using the Schwarz–Christoffel mapping for a sloped step.

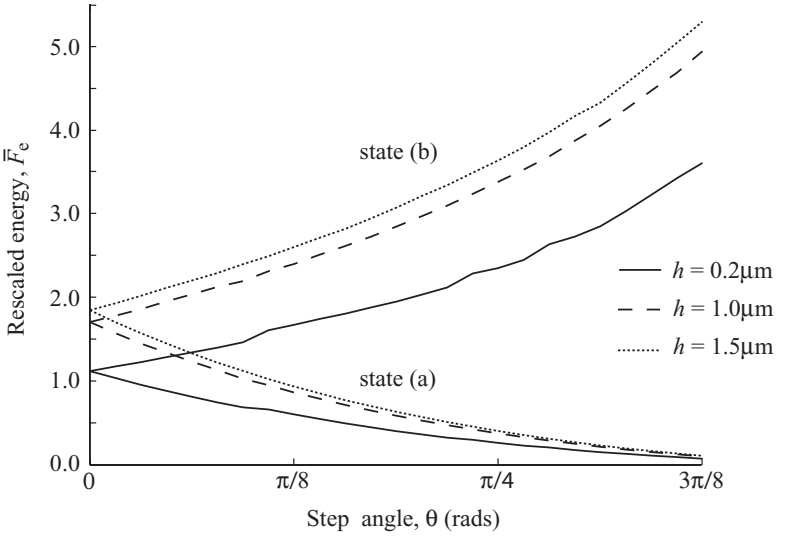

FIGURE 13. Rescaled elastic energy as a function of step angle θ, for different step heights and for states (a) and (b) from Figure 12.

in equation (4.1). We use the numerical procedure described earlier to evaluate ϕ within the domain. For example, with a tilt angle of $\theta = \pi/4$ we can produce two different director profiles by setting the boundary conditions as: (a) $\phi_1 = 0$, $\phi_2 = -\pi/4$ and $\phi_3 = 0$ and (b) $\phi_1 = 0$, $\phi_2 = \pi - \pi/4$ and $\phi_3 = 0$, as shown in Figure 12.

As in the previous section, the elastic energy of each state will be dependent on the height of the step h. Now, however, the energy will also depend on the step angle θ. We have numerically integrated the elastic energy density (again avoiding the regions close to the defects at the step corners) and the rescaled elastic energy is plotted in Figure 13 as a function of θ and for a number of values of h and for the two states shown in Figure 12.

Figure 13 indicates that only when the step is vertical (i.e. $\theta = 0$) do the two states have the same total energy, regardless of the value of h. This is in agreement with the analytic

https://doi.org/10.1017/S0956792510000380 Published online by Cambridge University Press

FIGURE 14. A typical periodic grating structure, which can support several stable director states.

prediction from the previous section. As θ increases the difference in energy between the two states always increases, with state (a) being energetically more favourable. This result is intuitive since an increase in step angle will tend to reduce the elastic energy of state (a), in the limit $\theta \to 0$ the elastic energy of state (a) will go to zero since there is no difference in director orientation across the step corner. Whereas, for state (b) a residual elastic energy contribution will remain even in the limit $\theta \to 0$. The increase in elastic energy for state (b) is harder to explain since, as θ increases, the defects at each of the step corners move apart, which would tend to decrease the elastic energy. However, there is also an increase in elastic energy as θ increases due to the region close to the bottom corner of the step (at $y = 0$). In this region, as θ increases, the director must rotate by an increasing amount, by an angle $\pi/2 + \theta$.

4.2 Periodic gratings

One device structure that has recently been examined experimentally is shown in Figure 14 [17]. In this structure one or both sides of the device have a periodic 'sawtooth' structure. Experimental results have shown a number of different stable director states. As indicated in previous work [17], the application of conformal mapping techniques can lead to a number of different director profiles (by altering the boundary conditions as in previous sections). To compare to experimental results a simple model of the optical transmission between crossed polarisers is used, where the transmission is given by

$$T = \sin^2(2(\chi + \theta)) \sin^2\left(\frac{\delta}{2}\right). \tag{4.2}$$

Here T is the relative optical transmission, taking values between 0 and 1, the angle χ is the angle between one of the crossed polarisers and the x-axis, and δ is the optical retardation of the liquid crystal layer defined as

$$\delta = \frac{2\pi n_\perp}{\lambda}\left(\frac{n_\perp}{n_\parallel} - 1\right), \tag{4.3}$$

where λ is the wavelength of the incident light and $n_\parallel$ and $n_\perp$ are the extraordinary and ordinary refractive indices of the liquid crystal used in the experiments.

As can be seen in Figure 15, the theoretical results, (b), compare well with the experimental results, (c). This technique therefore provides a fast and reliable method to determine the director profile of any given experimental state.

Using the conformal mapping method we are also able to predict the existence of many other potentially stable configurations which have not been observed experimentally but,

https://doi.org/10.1017/S0956792510000380 Published online by Cambridge University Press

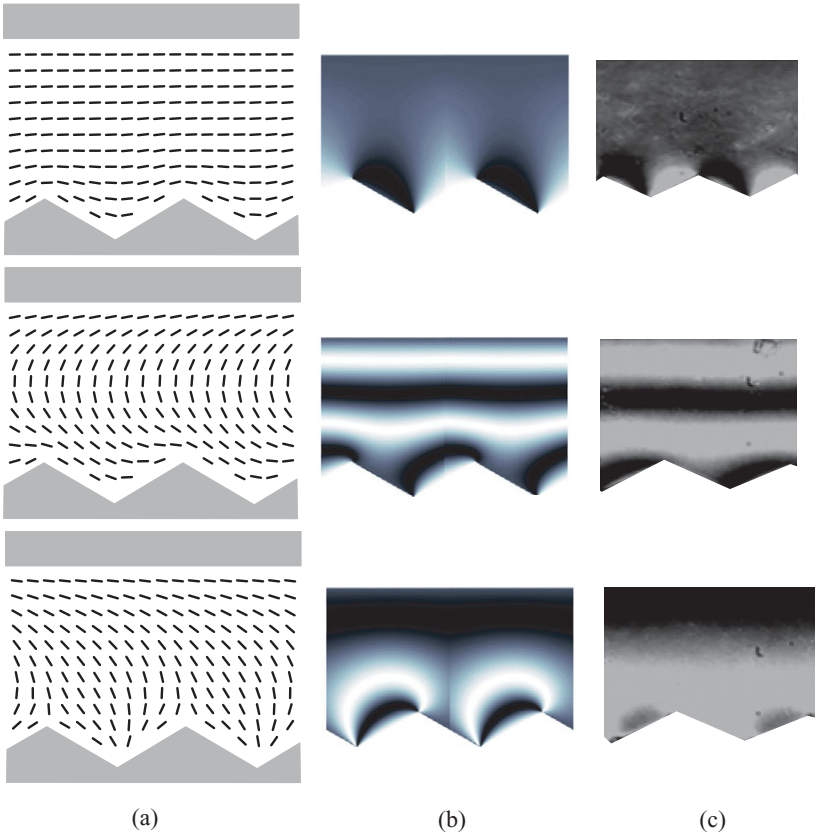

FIGURE 15. (Colour online) (a) The director profile produced using the Schwarz–Christoffel conformal map, (b) optical transmission between crossed polarisers of the theoretical director profiles in (a) and (c) Experimental optical textures from a similar device between crossed polarisers (optical textures courtesy of C.R. Evans).

if these undiscovered states have favourable optical characteristics, may lead to further experimentation to discover them.

4.3 Defect movement in confined geometries

One further example of the use of the Schwarz–Christoffel mapping is to investigate defect motion. For this example we use a recently developed bistable display [20], which uses a confining square geometry to produce two stable states, each of which has two defects located close to corners of the square, see Figures 16(a) and (e). In Ref. [26], a comparison between experimental results and theoretical predictions was given. In switching between these two states it was observed experimentally that the defects move between corners but remain close to the edges of the square. It is therefore possible to mimic this switching process using the Schwarz–Christoffel mapping. In changing from state (a) to state (e) in Figure 16 it is clear that only the boundary condition on the edge connecting point A to point B has been changed. We may perform this change by introducing an additional

https://doi.org/10.1017/S0956792510000380 Published online by Cambridge University Press

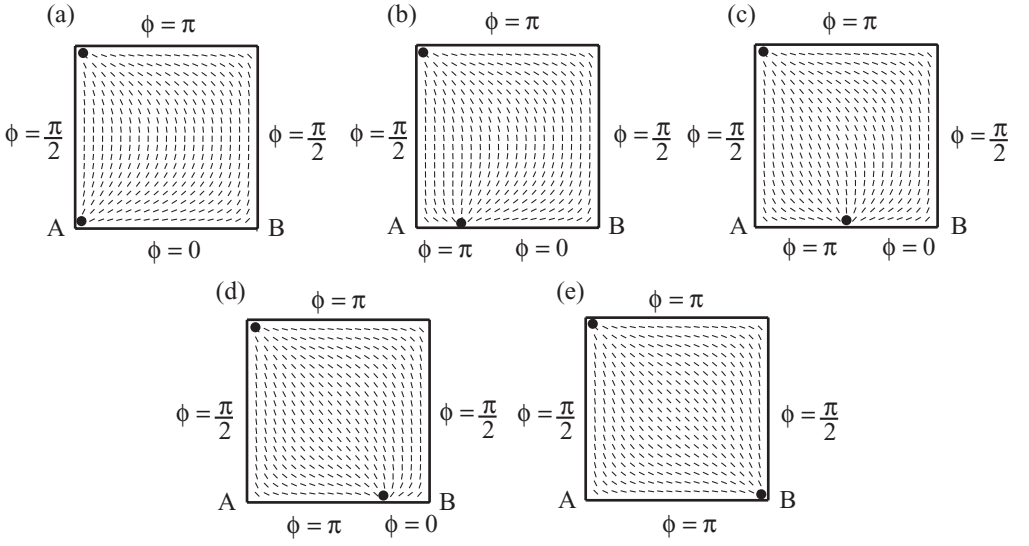

FIGURE 16. Director profiles as a defect is moved along one edge from A to B. States (a) and (e) are stable.

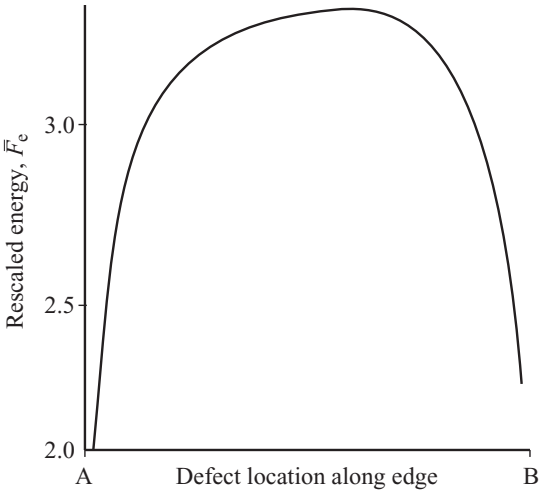

FIGURE 17. Rescaled energy as a function of defect position.

defect, a point where the boundary condition changes between A and B, and then alter the position of this defect. This additional point along AB becomes an additional apex of the polygon which is mapped to the upper half-plane through the Schwarz–Christoffel mapping and the process of calculating the director orientation and the energy of each state remains the same as in previous sections.

The rescaled energy as a function of defect position is calculated numerically and is shown in Figure 17. From this plot it is clear that local energy minima occur when the defect is at A or B, i.e. states (a) and (e) in Figure 16.

https://doi.org/10.1017/S0956792510000380 Published online by Cambridge University Press

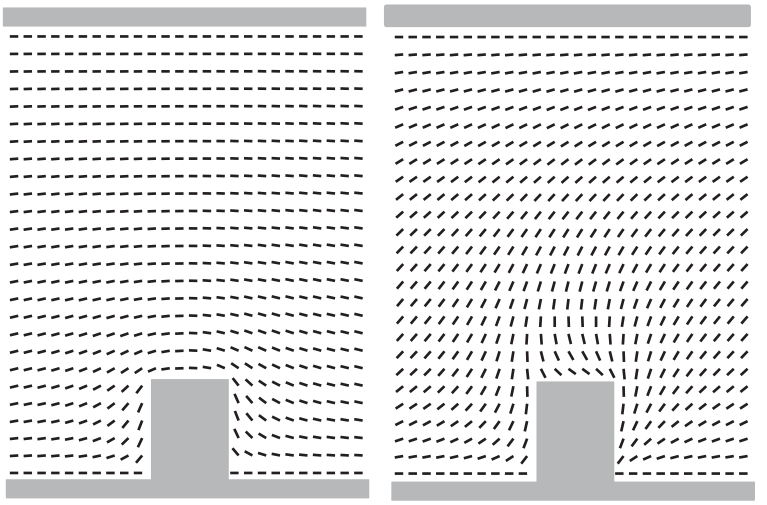

FIGURE 18. Two stable director profiles for the PABN device.

This approach may be of use in the development of a number of bistable display technologies, which work on the principle of moving defects in a given geometry from one place to another, thus switching between stable states.

5 Director configurations as initial conditions

The results of the conformal mapping technique necessarily assume that the splay and bend elastic constants are equal, i.e. $K_1 = K_3$. Further approximation is implicit in the fact that defects may not occur in the interior of the liquid crystal domain and defects which are present at corners of a polygonal domain may, in reality, be unstable to a variety of possible perturbations of the system. To obtain more accurate results, the director profile from a conformal mapping can be used as an initial condition in a more accurate theoretical setting such as the Q-tensor model [28]. Similar construction of initial states, in a three-dimensional model, have also been investigated in Ref. [19]. In this type of model, the orientational order of the liquid crystal material is also included as a dependent variable and a fuller description of defects is possible, allowing the possibility of motion of the defects to attain a lower energy state. Less stringent assumptions on the material parameters are possible in such a model and many experimentally determined parameters for a specific liquid crystal material can be used. In addition, since the cores of defects can be more accurately modelled, the energy of each state can be calculated to a higher degree of accuracy. A more detailed examination using the Q-tensor method has been presented in Refs. [11,17].

Two examples of bistable displays which use the motion of defects to switch between states are the PABN [16] and ZBD [6] displays. Both of these displays have been modelled successfully using a Q-tensor approach and finite element methods but such simulations are computationally expensive and time consuming. One time-consuming aspect of the simulation is the creation of accurate initial conditions. However, using the conformal mapping techniques these can quickly be produced. In the case of the PABN device,

https://doi.org/10.1017/S0956792510000380 Published online by Cambridge University Press

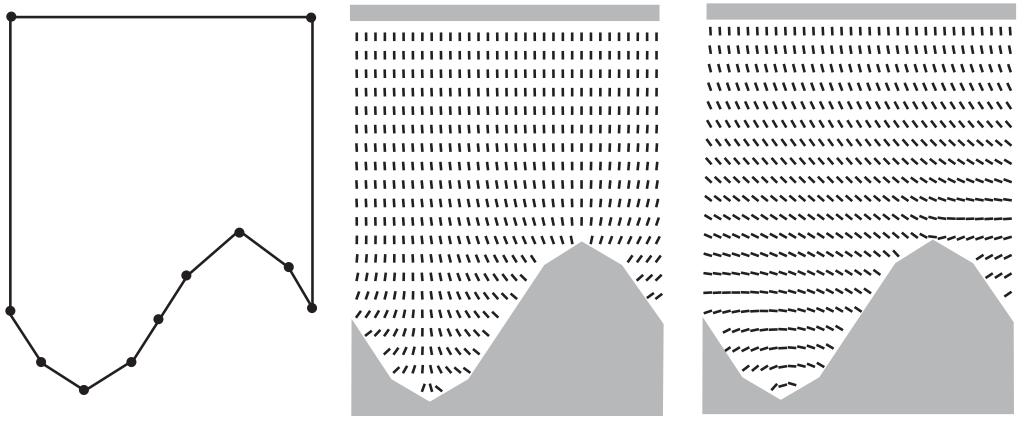

FIGURE 19. Two stable director profiles for the ZBD display.

a simple model, which considers the post structures which produce bistability as two-dimensional structures can be constructed. For this situation, two different stable states can be found, as shown in Figure 18, with the use of suitable boundary conditions. Using such a solution as the initial condition for a Q-tensor based approach, with a finite element method solver, allows optimisation of the cell geometry, i.e. by varying the height and width of the post.

A further limitation to the conformal mapping method described so far in this paper is the restriction to polygonal geometries. Although it is possible to construct conformal maps of domains which are bounded by arcs of circles and linear elements, in general we have found it useful to approximate a general substrate structure using only line elements, increasing the number of line elements to increase the accuracy. To model the ZBD display for instance, a smooth lower substrate can be approximated using line segments as shown in Figure 19.

The Schwarz–Christoffel method can then be used to calculate the director profile for two states as shown in Figure 19. As mentioned previously, we can then use these director profiles as initial conditions in a finite element method solver to reduce the time required to find the equilibrium state within a Q-tensor model.

6 Conclusions

In this paper we have demonstrated the use of conformal mapping techniques to model various two-dimensional liquid crystal filled geometries. Because of the rotational degeneracy of the nematic director several different stable states can be found and their energies can be compared. Conventional modelling of complex geometries often use computationally intensive numerical methods. The conformal mapping method, by comparison, takes a relatively short time to produce an accurate director profile for a given geometry. We have also shown that it is also possible to model the (quasi-static) switching between states if during the transition defects remain close to the domain boundary. The director configurations can be used to identify experimentally produce optical textures and to optimise device geometries, using the comparison of energies of different states.

https://doi.org/10.1017/S0956792510000380 Published online by Cambridge University Press

Acknowledgements

The authors are grateful for funding from the Engineering and Physical Sciences Research Council, for many fruitful discussions with Prof. Carl Brown and Dr Carl Evans, and for their permission to use the experimental images in Figure 15.

References

[1] Atluri, S. N. & Zhu, T. (1998) A new meshless local petrov-galerkin (MLPG) approach in computational mechanics. *Comput. Mech.* **22**, 117–127.
[2] Barberi, R., Martinot-Lagarde, P., Durand, G. & Giocondo, M. (1994) U.S. Patent No. 5357358.
[3] Barbero, G. (1981) On the critical angle of a NLC cell. *Lett. Nuovo Cimento* **32**, 60–64.
[4] Barbero, G. & Scaramuzza, N. (1982) On the interface substrate-nematic - anchoring energy and topography. *Lett. Nuovo Cimento* **34**, 173–179.
[5] Bartolino, R., Li, J., Barberi, R., Dozov, I., Durand G. & Giocondo M. (1999) U.S. Patent No. 5995173.
[6] Bryan-Brown, G. P., Brown, C. V. & Jones, J. C. (1995) UK patent GB2318422.
[7] Bryan-Brown, G. P., Brown, C. V. & Jones, J. C. (2001) U.S. Patent No. 6249332.
[8] Carbone, G., Lombardo, G. & Barberi, R. (2009) Mechanically induced biaxial transition in a nanoconfined nematic liquid crystal with a topological defect. *Phys. Rev. Lett.* **103**, 167801.
[9] Clark, N. A. & Lagerwall, S. T. (1980) Submicrosecond bistable electro-optic switching in liquid-crystals. *Appl. Phys. Lett.* **36**, 899–901.
[10] Davidson, A. J. & Mottram, N. J. (2002) Flexoelectric switching in a bistable nematic device. *Phys. Rev. E* **65**, 051710.
[11] Davidson, A. J., Brown, C. V., Mottram, N. J., Ladak, S. & Evans, C.R. (2010) Defect trajectories and domain-wall loop dynamics during two-frequency switching in a bistable azimuthal nematic device. *Phys. Rev.* E **81**, 051712.
[12] Driscoll, T. A. & Trefethen, L. N. (2002) *Schwarz-Chrtistoffel Mapping*, Cambridge University Press, Cambridge, UK.
[13] Dozov, I. & Durand, G. (1999) Surface controlled nematic bistability. *Pramana-J. Phys.* **53**, 25–35.
[14] de Gennes, P. G. & Prost, J. (1993) *The Physics of Liquid Crystals,* 2nd ed., Clarendon Press, Oxford.
[15] Ivanov, V. I. & Trubetskov, M. K. (1995) *Handbook of Conformal Mapping with Computer-Aided Visualization*, CRC Press, Boca Raton, USA.
[16] Kitson, S. & Geisow, A. (2002) Controllable alignment of nematic liquid crystals around microscopic posts: Stabilization of multiple states. *Appl. Phys. Lett.* **80**, 3635–3637.
[17] Ladak, S., Davidson, A. J., Brown, C. V., & Mottram, N. J. (2009) Sidewall control of static azimuthal bistable nematic alignment states. *J. Phys.* D - *Appl. Phys.* **42**, 085114.
[18] Lagerwall, S. T. (1999) *Ferroelectric and Antiferroelectric Liquid Crystals*, Wiley, New York.
[19] Majumdar, A., Newton, C. J. P., Robbins, J. M. & Zyskin, M. (2007) Topology and bistability in liquid crystal devices. *Phys. Rev.* E **75**, 051703.
[20] Mottram, N. J., Ramage, A., Kelly, G. & Davidson, A. J. (2006) UK patent GB20040026582.
[21] Newton, C. J. P. & Spiller, T. P. (1997) Bistable nematic liquid-crystal device modeling. In: *SID Proceedings of IDRC '97 SID,* Santa Ana, CA, USA, pp. 13–16.
[22] Schopohl, N. & Sluckin, T. J. (1987) Defect core structure in nematic liquid-crystals. *Phys. Rev. Lett.* **59**, 2582–2584.
[23] Spencer, T. J. & Care, C. M. (2006) Lattice boltzmann scheme for modeling liquid-crystal dynamics: Zenithal bistable device in the presence of defect motion. *Phys. Rev. E* **74**, 061708.
[24] Spiegel, M.R. (1964) *Complex Variables with an Introduction to Conformal Mapping and its Applications*, Schaum's Outlines Series, McGraw-Hill.

[25] Towler, M. J., Bryan-Brown, G. P., McDonnell, D. G. & Brancroft, M. S. (1999) U.S. Patent No. 5796459.
[26] Tsakonas, C., Davidson, A. J., Brown, C. V. & Mottram, N. J. (2007) Multistable alignment states in nematic liquid crystal filled wells. *Appl. Phys. Lett*. **90**, 111913.
[27] Uche, C., Elston, S. J. & Parry-Jones, L.A. (2006) Modelling zenithal bistability at an isolated edge in nematic liquid crystal cells. *Liq. Cryst*. **33**, 697–704.
[28] Wojtowicz, P. J., Priestly, E. B. & Sheng, P. (1976) *Introduction to Liquid Crystals*, Plenum Press, New York and London.

https://doi.org/10.1017/S0956792510000380 Published online by Cambridge University Press